Published in final edited form as:

Spectrochim Acta Part B At Spectrosc. 2020 June ; 168: . doi:10.1016/j.sab.2020.105871.

A predictive model for elemental carbon, organic carbon and total carbon based on laser induced breakdown spectroscopy measurements of filter-collected diesel particulate matter

R.P. McLaughlin[a,*], **D.A. Parks**[b], **A.I. Grubb**[c], **G.S. Mason**[d], **A.L. Miller**[b]

[a]Department of Chemistry, Seattle University, Seattle, Washington 98122, USA

[b]National Institute for Occupational Safety and Health (NIOSH), Spokane, Washington 99207, USA

[c]Department of Physics, San Diego State University, San Diego, California 92182, USA

[d]Department of Mechanical Engineering, Seattle University, Seattle, Washington 98122, USA

1. Introduction

Diesel particulate matter (DPM) produced from vehicle and equipment diesel exhaust (DE) is a common industrial inhalation hazard, particularly in underground mines [1–3]. The sub-micron particles of DPM (< 800 nm) are composed of a carbonaceous core operationally defined as elemental carbon (EC), which are irregularly arranged graphitic-like “spherule” structures, and a wide-variety of adsorbed, semi-volatile organic carbon compounds (OC) [3]. In addition to associating chronic exposure to DPM with immunological, respiratory and cardiovascular health issues, the International Agency for Research on Cancer (IARC) categorizes this material as carcinogenic to humans, with workers regularly exposed to it demonstrating an elevated risk for lung cancer [4–6]. Given the long-term health risks associated with repeated and prolonged exposure to DPM, efforts are being directed at reducing the exposure of miners and other workers who may encounter high levels of DPM over the course of a typical working day [7].

New technologies are being developed to reduce airborne DPM levels through a reduction in engine emissions, including advanced engine designs, a host of after-treatment systems, and a variety of alternative fuels [8–11]. The latter have been shown to markedly decrease respirable DPM and other hazardous components of DE from mining vehicles [11], yet high exposures persist, most prevalently in underground mines. The Mine Safety and Health Administration (MSHA) has set a time-weighted average (TWA) DPM exposure limit of 160 $\mu g/m^3$ based on total carbon (TC, defined as the sum of EC and OC) and a cut-point of 800 nm for TC particle size [12].

*Corresponding author. mclaughlinr@seattleu.edu (R.P. McLaughlin).

CRediT author statement

All authors contributed in the same way towards completion of this article.

Declaration of Competing Interest

The authors declare that they have no known competing financial interests or personal relationships that could have appeared to influence the work reported in this paper.

Reducing occupational exposure to DPM is aided by measuring the levels of this airborne hazard in active work settings. In mines, exposures to DPM are often measured by collecting air samples onto filters (usually full-shift samples) and sending them to external laboratories for analysis using a thermo-optical method such as the NIOSH Standard Method 5040 [13]. Method 5040 is designed to quantify the mass of EC and OC present, which is, in turn, used to determine the concentration of DPM in the sampled air. The EPA-IMPROVE method also uses a thermal evolution approach but goes a step further by breaking OC into several distinct groups [14]. While these methods have been shown to be accurate in determining the amount of OC, EC and TC present, they both have the significant limitation of being off-site laboratory methods, typically resulting in a time-span of days to weeks to complete the collection and analysis cycle. This limitation hampers mine safety personnel in efficiently utilizing air quality results to plan DPM reduction strategies and, more importantly, in responding to potentially rapidly changing working conditions.

Some previously established techniques have been shown to quantitate EC [15] in mine atmospheres, and in some cases, EC can be used as a surrogate for DPM; however, this assumes a constant EC-to-OC ratio. While it has been shown that the air in some mines has consistent and constant EC/OC ratio, that is not always the case [16,17] since the ratio can vary due to four issues: (1) in most mines, a variety of diesel-powered equipment is used, and each piece of equipment has a different engine, which have different emission profiles (EC/OC ratios) even when the same fuel is being used, (2) engine load and fuel types are variable, (3) the use of aftertreatment methods vary, and (4) the presence of cigarette smoke, oil mist, paint spray, or blast fumes may elevate the OC. Each of these factors leads to a variability of EC/OC ratios in the air, in both time and space [18], making it difficult to compare real-time indications of EC with TWA measurements of DPM/TC over a work shift, which is how the levels of DPM are measured for regulatory purposes.

Laser-induced Breakdown Spectroscopy (LIBS), an atomic emission technique capable of both qualitative and quantitative analysis, has been utilized previously to determine concentrations of airborne particulate matter [19–24]. The LIBS method provides an intriguing option for studies such as these due to its high sensitivity and rapid measurement capabilities. Although LIBS does not directly distinguish between EC and OC from the elemental carbon emissions present in the plasma plume, the broad-band spectral acquisition capabilities of this technique, and its ability to measure multiple elemental emissions simultaneously, suggest an intriguing avenue to explore, particularly when the LIBS data is coupled with chemometric modeling methods. In this study, a partial least squares (PLS) regression model was generated from LIBS spectra and Method 5040 data derived from DPM samples collected on quartz fiber filters to evaluate the effectiveness of LIBS measurements in predicting OC, EC, and TC in air samples. In accordance with previous work [25–27], the validity of the PLS models was characterized using root-mean-squared error of calibration (RMSEC), cross-validation (RMSECV) and prediction (RMSEP), the coefficients of determination, R^2, for calibration and prediction, the range error ratio (RER), and the residual prediction to the standard deviation (RPD). The results provided here suggest that LIBS measurements coupled with PLS modeling represents a promising direction for the rapid analysis of DPM concentrations.

2. Methods

2.1. DPM production and sampling

To simulate the evolving nature of DPM in the workplace, specifically a potentially more diverse array of OC/EC ratios, the forty-nine samples produced for this study were collected from the tailpipe of a Robin DY42 diesel engine using three different engine loads (3 kW, 4 kW and 5 kW). The loads were provided by a 6 kW genset (Generator set: Pow'R Gard Model: DG6E) attached to a resistive load bank. The samples were generated using a lab-based collection system, specifically designed for collecting tailpipe samples from a variety of diesel engines. The system, illustrated in Fig. 1, consists of an insulated sampling tube, a dilutor, a quiescence chamber, and a multi-port sampling manifold.

Samples were collected by placing a sampling wand at the tailpipe exit. The wand was connected to a sampling tube that was insulated and fitted with heating tape to prevent premature condensation of volatile DPM aerosols. The hot stream of raw exhaust was drawn through the insulated sampling tube via the suction provided by the ejector-style dilutor, where it was instantly diluted with cool, dry air. The dilutor was configured to provide approximately a 10:1 dilution ratio. The secondary airflow exiting the dilutor was directed under slight pressure into a quiescence chamber. The chamber was regulated to ~49 Pa above atmospheric pressure by a separate fan and louvre control that jettisoned some pressurized air to the ambient atmosphere. The quiescence chamber was fitted with a 12-port manifold, with each port having a 1.7 l/min critical orifice as shown in Fig. 1. The vacuum supplied to the manifold was maintained at > 53 kPa to ensure critical flow through the orifices, using a vacuum pump.

Standard 37-mm quartz fiber filters in SKC cassettes (with 0.8-μm impactors) were used to collect the DPM. Even though Teflon filters are commonly used by the atmospheric chemistry community, quartz filters were used both because the Sunset Laboratory instrument used to provide primary OC and EC values requires (thermally stable) quartz filters, and because these filters are specified by MSHA in the regulatory method regarding quantification of worker exposure to DPM (both EC and OC). Samples were collected at various intervals for the different engine loads, with the longest collection time being 2 h.

2.2. NIOSH standard method 5040 analysis

As a baseline against which to compare the LIBS data, each sample was analyzed using a Sunset Laboratory Inc. Organic Carbon / Elemental Carbon (OCEC) Laboratory Instrument Model 5 L. The instrument was used to measure organic and elemental carbon according to Method 5040. A description of this method can be found in previous work [28,29]. In brief, it is a thermo-optical method, where EC and OC are operationally determined by applying heating cycles to the sample first in a helium (non-oxidative) environment and then in an oxidative environment. In both cases, the entrained carbon is oxidized to carbon dioxide, reduced to methane, and detected with a flame-ionization detector (FID). The non-oxidative cycle defines the OC mass while the oxidative process defines the EC mass. An optically determined correction to the split point between OC and EC evolution accounts for char, defined here as an amount of OC that is pyrolized to EC during the first heating cycle.

2.3. Laser induced breakdown spectroscopy measurements

The LIBS instrument used for this study is described in detail elsewhere [24]. Briefly, the instrument, shown schematically in Fig. 2, uses a Nd:YAG laser (MK-367,Kigre) and multi-channel spectrometer (Multichannel AVS-USB2, Avantes) to perform LIBS analysis on samples, and is capable of automated collection, deposition, and spectroscopic measurement of airborne particulate matter. On-board software performs the analysis of collected spectra and reports measured amounts through a touch-screen display. The spectrometer, triggered by the laser using a photodiode, was set to an integration delay of 1.16 μs and an integration time of 1 ms.

This instrument was designed as a “reel-to-reel” system; however, since comparison with the Method 5040 data required use of pre-collected samples on 37 mm filters, the LIBS instrument was modified to allow “manual analysis” of individual 37 mm filter samples, replacing the reel-to-reel collection head with another fixture designed to hold 37 mm filters. Following center punching of the filter for Method 5040 analysis, the remainder of the 37 mm filter with deposited DPM was removed from its cartridge and manually placed into the fixture (see Fig. 2 inset). The top section of the mount, which rests on the face of the sample filter, separates the surface of the filter into sixteen different measurable regions, allowing each sub-section to be probed by the LIBS system without redepositing ablated material onto unmeasured portions. The specialized mount allows numerous replicate measurements to be performed at a fixed distance from the center of the filter, but only one LIBS ablation shot was performed for each of the sixteen subsections. Particle deposition is taken to be essentially uniform due to the small size of DPM particles, and if minor inhomogeneities in sample deposition exist based on position, measuring samples at a fixed distance from the center of the filter, as was performed in this study, likely mitigates that variability. The sixteen collected spectra from a given sample are then averaged, and peak areas for relevant emission lines are determined. Previous work has stated uncertainties in LIBS emissions of around 10–15%, [23] primarily due to shot-to-shot variability in plasma temperatures and matrix inhomogeneities in the samples, and the same general range is expected here.

2.4. PLS modeling

The LIBS spectra and 5040 data for the 49 samples collected for this study were modeled using the PLS algorithm present in the Unscrambler software package (Camo Analytics, Woodbridge, NJ) to examine the relationships in the overall data set and to examine the potential predictive abilities of the LIBS data. The general PLS method is described in detail elsewhere [30,31]. Briefly, though, given a matrix **X** comprised of wavelength-dispersed LIBS intensities measured for known DPM samples (the rows of **X**), and a **Y** matrix formed from the Method 5040 determined loadings of EC, OC and TC of those same samples, the PLS method seeks a set of principal component factors that explain the variation in **X** while also producing a strong correlation with the data in **Y**. Such a regression seeks to produce a model that not only describes potential patterns and groupings in the set of independent variables **X**, but also provides good predictions of future unknown dependent variables in **Y.** There are numerous examples of applying PLS methods to LIBS measurements [32–37]. In this study, the sixteen-shot averaged spectrum for each sample was used as the spectral input for the PLS analysis. The wavelength range collected from the spectrometer was 190 nm to

800 nm spanning five different channels; however, sections of this spectral range containing primarily baseline were omitted from the model.

The DPM samples examined in this study were divided into a calibration set (twenty-seven samples) and a validation set (twenty-two samples) to explore the predictive abilities of the LIBS measurements. The calibration and validation sets were chosen so that representative samples from the three engine loads were included in each set, and, as much as possible, samples with a variety of collection times (and, thus, mass loading) were included in the two sets to more reasonably evaluate the predictive abilities of the model. Random cross-validation on twenty subsets of samples was performed on the calibration set, with one or two samples systematically removed from the calibration data set for each validation step and then the model created from the remaining samples used to predict the removed values. The cross-validation process was repeated for the other subsets, and a measure of the overall dispersion of the predicted values of the validation samples around the regression line (RMSECV) was determined. The cross-validated model was then used to predict the OC, EC and TC values of the twenty-two samples in the validation set.

3. Results/discussion

Method 5040 analysis results for the 49 DPM samples examined in this study are illustrated in Figs. 3 and 4. Fig. 3 is a plot of the loading ($\mu g/cm^2$) of EC and OC as determined by Method 5040 as a function of filter collection time for each of the three engine loads examined. As shown in this figure, the EC and OC values both increase with collection time for all the engine loads examined, and the OC component demonstrates more variability in the Method 5040 values. This set of plots also shows that the relative amount of OC to EC varies as a function of engine load, with the heaviest engine load (5 kW) producing approximately equal proportions of the two quantities and an overall greater mass load of DPM than the other engine loads (3 kW and 4 kW). The relative proportions of OC and EC for the three engine loads are illustrated in Fig. 4, a plot of OC as a function of EC. This figure demonstrates that the OC/EC ratio produced is different for the three engine loads, with heavier engine loads enriched in EC relative to the amount of OC present. However, within each engine load, the relationship between OC and EC is relatively consistent as shown by the least-squares fits. This latter result suggests the test conditions used in this study were reasonably repeatable. In Fig. 3, it is notable that the y-intercept is non-zero for some of the data. For EC this is due to errors inherent in the Method 5040 values, and for OC it is likely related to outgassing of the plastic cassettes using in the sampling process. This OC artifact could be overcome in future studies by using filter cassettes which have not begun approach their expiration date or by precleaning the quartz filters in a low temperature asher. However, given the aim was to replicate the NIOSH method 5040 regardless of how the carbon came to be on the quartz fiber filters, aerosol sampling was not the primary goal of this paper thus non-zero intercept for OC is not of consequence.

Fig. 5 illustrates representative LIBS spectra obtained for the 5 kW engine load over time. Carbon emissions at 193 nm, 229 nm, and 247 nm are observed to grow as deposition time increases. LIBS emission at these wavelengths should provide a measure of the total carbon present in the DPM samples. Most of the additional emission lines present in Fig. 5 originate

from the silicon present in the glass fiber filters, which remain essentially fixed in intensity with increased carbon load. Fig. 6 shows the integrated areas of the 193 nm carbon emission for the three engine loads plotted as a function of the TC amount (determined separately through Method 5040). Each carbon emission value in these plots is the average of sixteen shots on a given sample filter. The integrated 193 nm emission intensity for the different engine loads shows general agreement for comparable TC values, and a fit of the collective samples together gives an R^2 value of 0.93. However, given that the relative amounts of OC and EC vary for the different loads applied to the engine, as seen in Figs. 3 and 4, using a single emission calibration for TC may not be reliable. First, the plasma properties may be different for DPM samples collected under different engine loads. Second, the plasma properties may be inconsistent because the total mass collected on the samples differs between the engine loads, increasing from the 3 kW to the 5 kW samples. Furthermore, given that working environments will likely involve particulate matter arising from multiple loads on multiple engines, a univariate calibration is likely not the optimal approach for producing a representative calibration model for DPM. PLS analysis will make fuller use of the LIBS spectra collected from these samples and could potentially provide an option for modeling the Method 5040 defined OC, EC and TC simultaneously.

A PLS model with full cross validation was created from all 49 samples used in this study. The scores plot for the first two factors (out of four total) of this model, shown in Fig. 7, indicates three general clusters of data points representing the three different engine loads. The blank samples present in the model align best with samples from the lightest engine load and the least amount of EC. Cross-validation results for the full model suggest that the most accurate predictions should be for EC values (RMSECV of 1.9815, $R^2 = 0.978$), with comparable variability between OC (RMSECV of 3.8700, $R^2 = 0.851$) and, not surprisingly, TC (RMSECV = 3.8256, $R^2 = 0.971$), given that TC is the sum of OC and EC values.

To evaluate the predictive potential of LIBS data, the overall set of LIBS measurements was split into a calibration set (27 samples) to generate a model and a prediction set (22 samples) to test the model. The validity of the model produced from this subset of samples for EC, OC and TC was characterized using RMSEC, RMSEP, the R^2 values for calibration and prediction, RPD (where RPD = standard deviation of prediction set/RMSEP) and RER (where RER = (maximum $_{\text{reference value}}$ − minimum $_{\text{reference value}}$)/RMSEP). RPD values greater than 3 and RER values greater than 10 are considered indicators of a quality predictive model [25–27]. The model produced used four factors to explain the variance, and the values for the various evaluation metrics are summarized in Table 1. The coefficient of determination, R^2, for each of the modeled species are over 0.90, suggesting that the regression model describes the variance in observed values quite well. As generally expected, the values for RMSECV are somewhat higher than the RMSEC values. The smaller the difference between these two values the better, and with larger data sets for gathered DPM, this gap between the two will perhaps narrow further. Furthermore, the RMSEC for OC is the highest of the three-component species modeled for DPM, consistent with the data shown in Fig. 3. The RMSEP values for the prediction set showed similar results as for the cross-validation, with the model predicting EC better than OC and TC, and with TC slightly higher than OC. Given that most of the variability in the prediction is based on OC, it makes sense that these two latter values would be similar.

As shown in Table 1, the RPD and RER values calculated from the results of predicting OC, EC and TC for the 22 samples in the prediction set indicate that the modeling for EC and TC meet benchmarks indicated in previous publications for reasonable models [25–27]. However, the OC values for this metric do not meet this standard. These results suggest that the use of LIBS spectral data to estimate the EC and TC values represents a promising approach, but the variability in OC makes direct predictions for this quantity unreliable.

The regression coefficients for the model produced for the calibration set for TC, shown in Fig. 8, indicate that strong weight is given to the carbon emission lines at 193 nm, 229 nm, and 252 nm. Calcium emission lines at 393 nm and 396 nm are also positively correlated with the model, likely due to their presence as a lube oil additive. The silicon single emission at 212 nm, its multiple emission lines near 252 nm, 263 nm, and 412 nm, as well as the lines at 504 and 505 nm all have weak or negative regression coefficients, particularly in comparison to their occasionally quite strong intensity in the LIBS emission spectra. Furthermore, the strong oxygen emission at 777 nm is also negatively correlated with the model. That the regression coefficients for silicon and oxygen are negatively correlated in the model used for predicting OC, EC, and TC makes sense given that there is likely greater ablation of the glass fiber filter for lighter loads of DPM (and, therefore, less carbon) due to increased penetration depth of the laser into the filter surface. Interestingly, though, the emissions assigned to silicon at 390 nm and 288 nm show positive regression coefficients, opposite of the behavior that would be expected for this component. Future modeling on wider data sets may help clarify the contribution of these emission lines to the PLS model for DPM. Lastly, the regression coefficients for OC and EC (not shown) both have a similar appearance to TC (and each other) in terms of the behavior of emission lines described above, indicative of the relationship between these quantities defined by the Method 5040 method.

4. Conclusion

Diesel particulate matter generated at three different engine loads was collected onto quartz fiber filters and analyzed using the NIOSH Standard Method 5040 and LIBS with the goal of estimating the OC, EC and TC content of the collected samples. Tracking the loading of OC and EC over time indicated that the sampling system used to produce the DPM samples behaves in a consistent manner. More variability was observed in the OC loading over time than for EC, most likely due to the higher volatility of the OC compounds. The higher variability in OC loadings will be explored in more detail in subsequent studies with DPM and LIBS. Consistent with other work, higher engine loads were shown to produce more EC relative to OC. A calibration curve based on a single carbon emission line provided a reasonable fit of TC for DPM; however, modeling DPM using multivariate regression enables more complete use of the broad-spectrum capabilities of LIBS. A calibration model for predicting OC, EC and TC was generated with PLS, using LIBS spectra from DPM samples. The training set used slightly over half of the spectra collected, and cross-validation of this calibration model illustrated the same increased variability for OC over EC. The RPD and RER rubrics for evaluating the prediction results from this model illustrate satisfactory predictions for EC and TC, while lesser accuracy is expected for characterizing the amount of OC. Overall, the approach of using LIBS to estimate levels of OC, EC and TC appears

promising, suggesting this approach may represent a complementary analysis to Method 5040, or similar methods, for estimation of these quantities.

Acknowledgments

The authors thank the National Institute for Occupational Safety and Health and the College of Science and Engineering at Seattle University (including the endowed PACCAR Professorship for G. Mason) for their financial support. They also thank Dr. Andy Weakly for helpful advice regarding PLS modeling.

Disclaimer

The findings and conclusions in this paper are those of the authors and do not necessarily represent the official position of the National Institute for Occupational Safety and Health, Centers for Disease Control and Prevention. Mention of any company or product does not constitute endorsement by NIOSH.

References

[1]. Birch ME, Cary RA, Elemental carbon-based method for monitoring occupational exposures to particulate diesel exhaust, Aerosp. Sci. Technol 25 (1996) 221–241, 10.1080/02786829608965393.

[2]. Kagawa J, Health effects of diesel exhaust emissions–a mixture of air pollutants of worldwide concern, Toxicology 181–182 (2002) 349–353, 10.1016/s0300-483x(02)00461-4.

[3]. Australian Institute of Occupational Hygienists (AIOH), Position paper – Diesel Particulate Matter & Occupational Health Issues, https://www.aioh.org.au/documents/item/15, (2013).

[4]. Health Effects Institute, Diesel Exhaust: A Critical Analysis of Emissions, Exposure, and Health Effects, A Special Report of the institute's Diesel Working Group, Health Effects Institute, Cambridge, MA, 1995.

[5]. Intern. Agen. Res. on Cancer (WHO), IARC: Diesel engine exhaust carcinogenic. Press release, 2012 (2012), p. 213.

[6]. Attfield MD, Schleiff PL, Lubin JH, Blair A, Stewart PA, Vermeulen R, Coble JB, Silverman DT, The diesel exhaust in miners study: a cohort mortality study with emphasis on lung cancer, J. Nat. Cancer Institut 104 (11) (2012) 869–883, 10.1093/jnci/djs035.

[7]. Bugarski AD, Schnakenberg GH Jr., Hummer JA, Cauda E, Janisko SJ, Patts LD, Effects of diesel exhaust after treatment devices on concentrations and size distribution of aerosols in underground mine air, Environ. Sci. Technol 43 (2009) 6737–6743, 10.1021/es9006355. [PubMed: 19764243]

[8]. Fiebig F, Wiartalla A, Holderbaum B, Kiesow S, Particulate emissions from diesel engines: correlation between engine technology and emissions, J. Occup. Med. Toxicol 9 (2014) 6, 10.1186/1745-6673-9-6. [PubMed: 24606725]

[9]. Bugarski AD, Janisko S, Cauda EG, Noll JD, Mischler SE, Controlling Exposure to Diesel Emissions in Underground Mines, Society for Mining, Metallurgy, and Exploration, Englewood, CO, 2012, pp. 361–362 ISBN-13: 9780873353601.

[10]. Bugarski AD, Janisko SJ, Cauda EG, Patts LD, Hummer JA, Westover C, Terrillion T, Aerosols and criteria gases in an underground mine that uses FAME biodiesel blends, Ann. Occup. Hyg 58 (8) (2014) 971–982, 10.1093/annhyg/meu049. [PubMed: 25060241]

[11]. Lutz EA, Reed RL, Lee VST, Burgess JL, Occupational exposures to emissions from combustion of diesel and alternative fuels in underground mining—a simulated pilot study, J. Occup. Environ. Hyg 12 (3) (2015) 18–25, 10.1080/15459624.2014.987384.

[12]. Mine Safety Health Admin, 30 CFR 57 Diesel Particulate Matter Exposure of Underground metal and Nonmetal Miners, Federal Register, 2006 p. 28924–9012.

[13]. NIOSH, Elemental carbon (diesel particulate): Method 5040 (supplement issued 1/15/98), in: Cincinnati OH (Ed.), NIOSH Manual of Analytical Methods, 4th ed., U.S. Department of Health and Human Services, Public Health Service, Centers for Disease Control and Prevention, National Institute for Occupational Safety and Health, DHHS (NIOSH) Publication No. 94–113, 1994.

[14]. Chow JC, Watson JG, Crow D, Lowenthal DH, Merrifield TM, Comparison of IMPROVE and NIOSH carbon measurements, Aerosol Sci. Technol 2001 (34) (2001) 23–34, 10.1080/02786820119073.

[15]. Noll JD, Janisko S, Mischler S, Real-time diesel particulate monitor for underground mines, Anal. Methods 5 (2013) 2954–2963, 10.1039/C3AY40083B.

[16]. Barrett CA, Master Thesis: Continuous DPM Monitoring in Underground Mine Environments: Demonstration of Potential Options in the Laboratory and Field, Virginia Tech, 2018.

[17]. Swanson J, Kittelson D, Pui D, Watts W, Alternatives to the gravimetric method for quantification of diesel particulate matter near the lower level of detection, J. Air Waste Manage. Assoc 60 (10) (2010) 1177–1191, 10.3155/1047-3289.60.10.1177.

[18]. Khalek IA, Blanks MG, Merritt PM, Zielinska B, Regulated and unregulated emissions from modern 2010 emissions-compliant heavy-duty on-highway diesel engines, J. Air Waste Manage. Assoc 65 (8) (2015) 987–1001, 10.1080/10962247.2015.1051606.

[19]. Cremers DA, Radziemski LJ, Direct detection of beryllium on filters using the laser spark, Appl. Spectrosc 39 (1) (1985) 57–63.

[20]. Neuhauser RE, Panne U, Niessner R, Laser-induced plasma spectroscopy (LIPS): a versatile tool for monitoring heavy metal aerosols, Anal. Chim. Acta 392 (1999) 47–54, 10.1016/S0003-2670(99)00053-7.

[21]. Hanh DW, Lunden MM, Detection and analysis of aerosol particles by laser-induced breakdown spectroscopy, Aerosol Sci. Technol 33 (2000) 30–48, 10.1080/027868200410831.

[22]. Dotouquet C, Gallou G, Le Bihan O, Sirven JB, Dermigny A, Torralba B, Frejafon E, Monitoring of heavy metal particle emission in the exhaust duct of a foundry using LIBS, Talanta 127 (2014) 75–81, 10.1016/j.talanta.2014.03.063. [PubMed: 24913859]

[23]. Stipe CB, Miller AL, Brown J, Guevara E, Cauda E, Evaluation of laser-induced breakdown spectroscopy (LIBS) for measurement of silica on filter samples of coal dust, Appl. Spectrosc 66 (11) (2012) 1286–1293, 10.1366/12-06671. [PubMed: 23146184]

[24]. McLaughlin RP, Mason GS, Miller AL, Stipe CB, Kearns JD, Prier MW, Rarick JD, Note: a portable laser induced breakdown spectroscopy instrument for rapid sampling and analysis of silicon-containing aerosols, Rev. Sci. Instrum 87 (2016) 056103, 10.1063/1.4949506. [PubMed: 27250478]

[25]. Williams P, Sobering D, Davies AMC, Williams P (Eds.), Near Infrared Spectroscopy: The Future Waves, NIR Publications, Chichester, UK, 1996ISBN-13: 978–0952866602.

[26]. Malley DF, Yesmin I, Eilers RG, Rapid analysis of hog manure and manure-amended soils using near-infrared spectroscopy, Soil Sci. Soc. Amer. J 66 (5) (2002) 1677–1686, 10.2136/sssaj2002.1677.

[27]. Lorenzo C, Garde-Cerdán T, Pedroza MA, Alonso GL, Salinas MR, Determination of fermentative volatile compounds in aged red wines by near infrared spectroscopy, Food Res. Int 42 (9) (2009) 1281–1286, 10.1016/j.foodres.2009.03.021.

[28]. Birch ME, Monitoring of diesel particulate exhaust in the workplace, NIOSH Manual of Analytical Methods (NMAM), 2154 2003.

[29]. Birch ME, Elemental carbon (diesel particulate): method 5040, NIOSH Manual of Analytical Methods (NMAM), 1999.

[30]. Haaland DM, Thomas EV, Partial least-squares methods for spectral analyses. 1. Relation to other quantitative calibration methods and the extraction of qualitative information, Anal. Chem 60 (1988) 1193–1202, 10.1021/ac00162a020.

[31]. Wold S, Sjöström M, Eriksson L, PLS-regression: a basic tool of chemometrics chemometrics and Intell, Lab. Syst 58 (2001) 109–130, 10.1016/S0169-7439(01)00155-1.

[32]. Martelli M, Brygo F, Sadoudi A, Delaporte P, Barron C, Laser-induced breakdown spectroscopy and chemometrics: a novel potential method to analyze wheat grains, J. Agric. Food Chem 58 (2010) 7126–7134, 10.1021/jf100665u. [PubMed: 20499936]

[33]. Martin MZ, Labbe N, Rials TG, Wullschleger SD, Analysis of preservative-treated word by multivariable analysis of laser-induced breakdown spectroscopy spectra, Spectrochim. Acta B 60 (2005) 1179–1185, 10.1016/j.sab.2005.05.022.

[34]. Martin MZ, Mayes MA, Heal KR, Brice DJ, Wullschleger SD, Investigation of laser-induced breakdown spectroscopy and multivariate analysis for differentiating inorganic and organic C in a variety of soils, Spectrochim. Acta B 87 (2013) 100–107, 10.1016/j.sab.2013.05.026.

[35]. Stipe CB, Hensley BD, Boersema JL, Buckley SG, Laser-induced breakdown spectroscopy of steel: a comparison of univariate and multivariate calibration methods, Appl. Spectrosc 64 (2) (2010) 154–160, 10.1366/000370210790619500. [PubMed: 20149276]

[36]. Clegg SM, Sklute E, Dyar M, Barefield JE, Wiens RC, Multivariate analysis of remote laser-induced breakdown spectroscopy spectra using partial least squares, principal component analysis, and related techniques, Spectrochim. Acta B 64 (2009) 79, 10.1016/j.sab.2008.10.045.

[37]. Amdar-Hernandez J, Garcia-Ayuso LE, Fernandez-Romero JM, Luque de Castro MD, Partial least squares regression for problem solving in precious metal analysis by laser induced breakdown spectrometry, J. Anal. At. Spectrom 15 (2000) 587, 10.1039/B000813N.

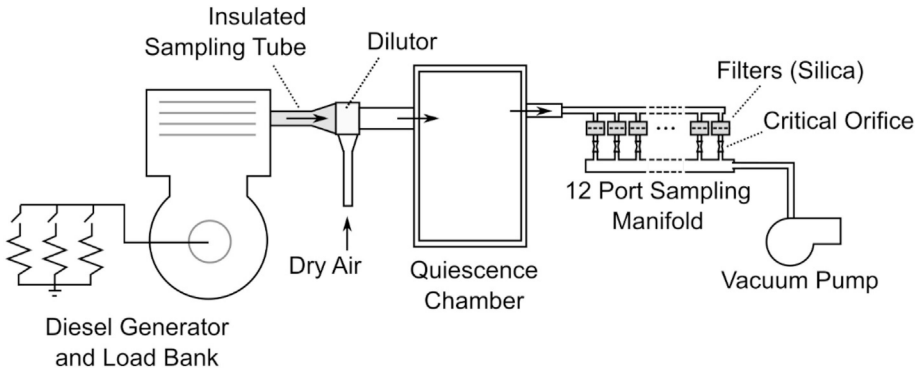

Fig. 1.

An illustration of the sampling arrangement used in this study, with a diesel generator and load bank to represent an operating (loaded) engine.

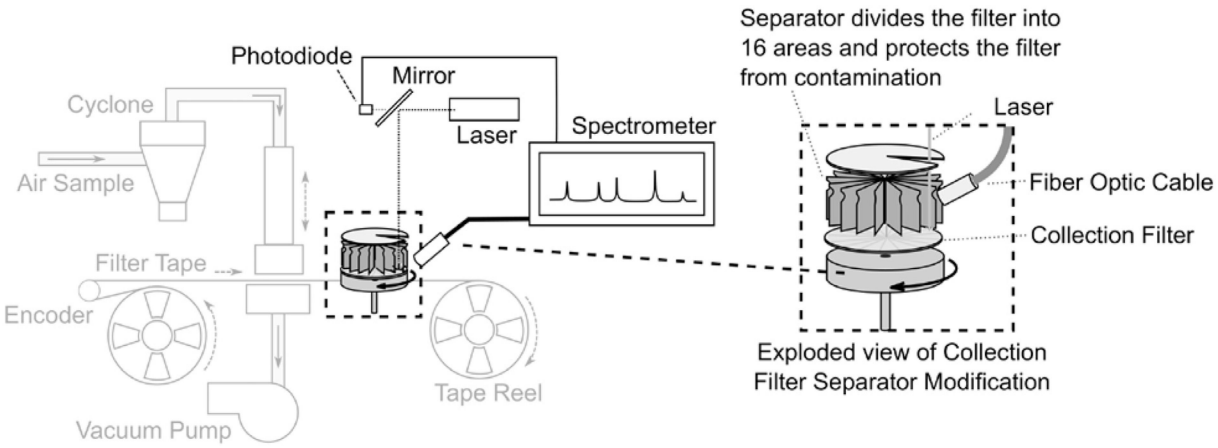

Fig. 2.

Schematic of LIBS instrument illustrating collection and analysis components, including filter separator (inset) that allows for sixteen shots to be taken on a single 37 mm filter without contamination from the deposition of ablated material. The reel-to-reel system (shown in light gray), which is used in other work for the collection and analysis of materials sampled from the environment, was removed and replaced with the filter separator for this current study.

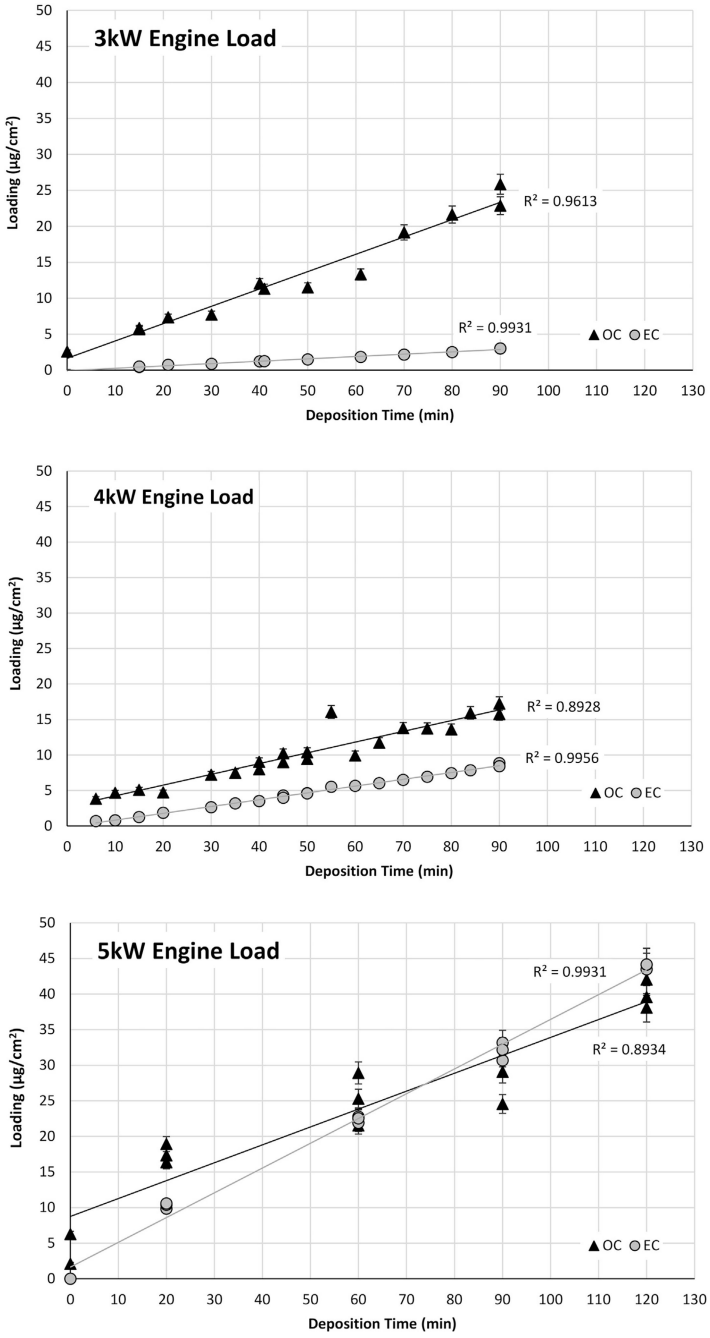

Fig. 3.

Plots illustrating EC (circles) and OC (triangles) mass loadings (μg/cm^2), as determined by the NIOSH 5040 method, as a function of time for three different engine loads: 3 kW (top), 4 kW (middle) and 5 kW (bottom). The error bars are obtained from the Sunset Laboratories Inc. OCEC instrument specifications and are taken to be ± 0.1 μg/cm^2 for loadings of less than 1.0 μg/cm^2 and ± 5% for heavier loadings.

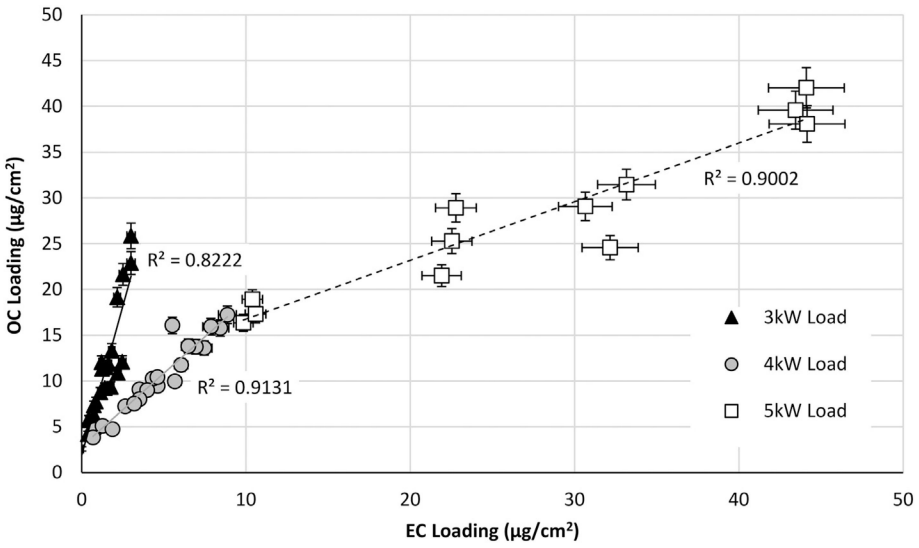

Fig. 4.

OC values plotted as a function of EC loading for three different engine loads. The error bars are obtained from the Sunset Laboratories Inc. OCEC instrument specifications and are taken to be ± 0.1 μg/cm^2 for loadings of less than 1.0 μg/cm^2 and ± 5% for heavier loadings.

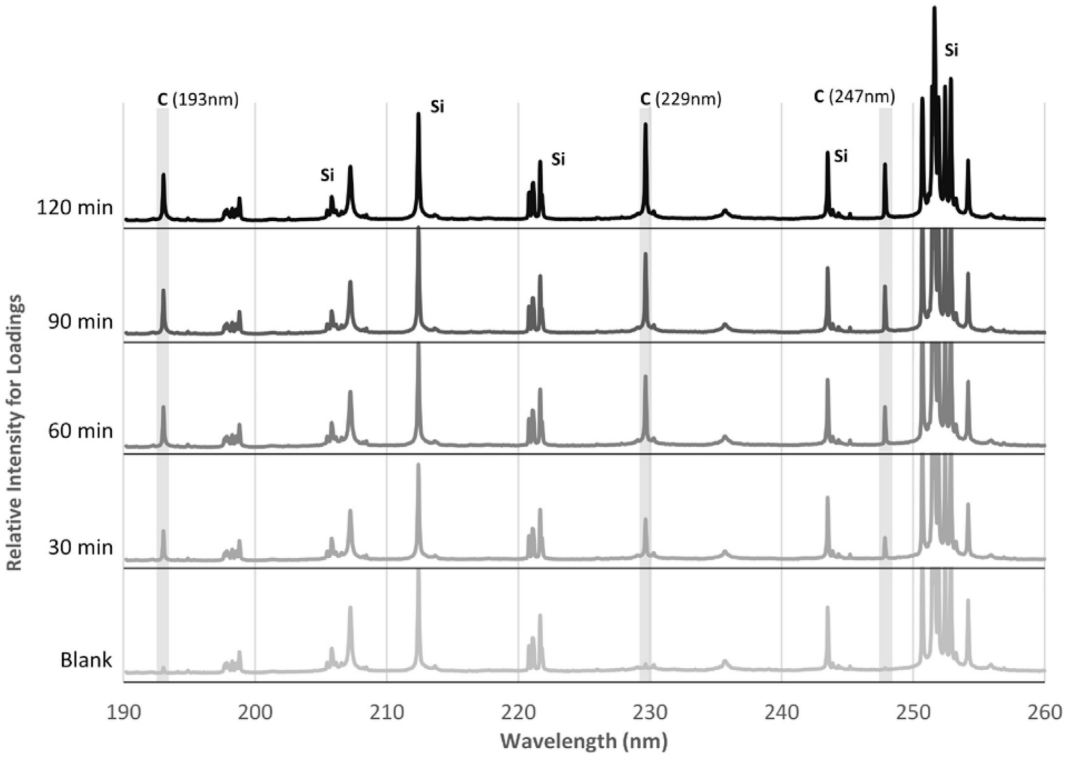

Fig. 5.

Portion of LIBS spectra obtained from 5 kW engine load and four different collection times (in addition to a blank filter at bottom). Most of the emission lines shown here are silicon transitions from the glass fiber filters.

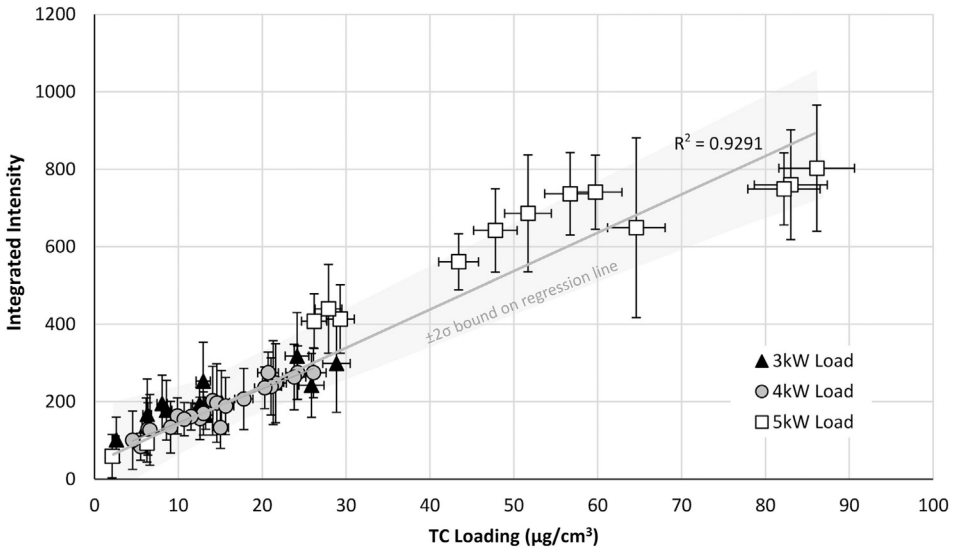

Fig. 6.

The 193 nm integrated emission intensity from carbon as a function of the 5040 determined values for TC for three different engine loads. The fit of the collective data has R^2 = 0.9291. The vertical error bars are produced from the standard deviation of the integrated 193 nm emission areas for the sixteen LIBS shots collected for each of the measured filters. The horizontal error bars are obtained from the Sunset Laboratories Inc. OCEC instrument specifications and are taken to be ± 0.1 μg/cm^2 for loadings of less than 1.0 μg/ cm^2 and ± 5% for heavier loadings.

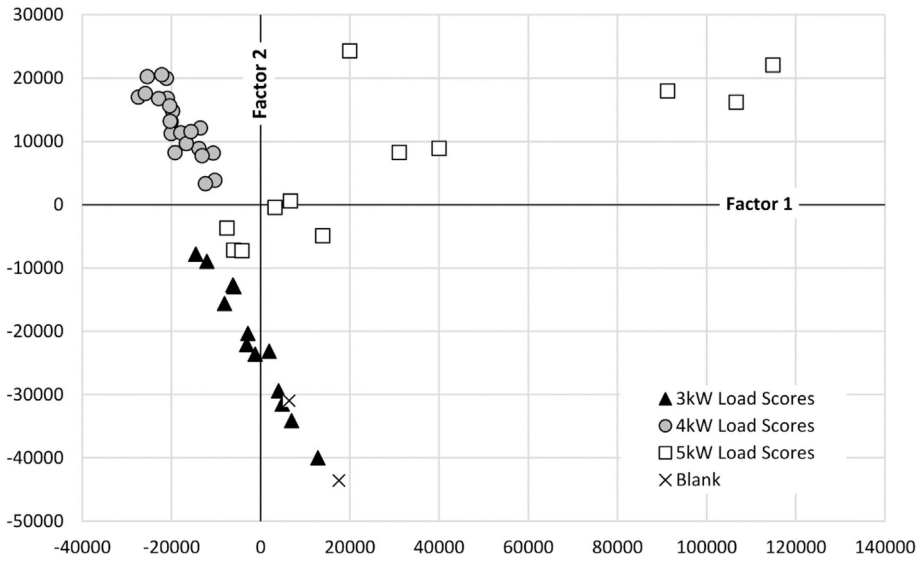

Fig. 7.

Scores plot from PLS analysis of the DPM LIBS spectra for all 49 samples collected, covering three different engine loads.

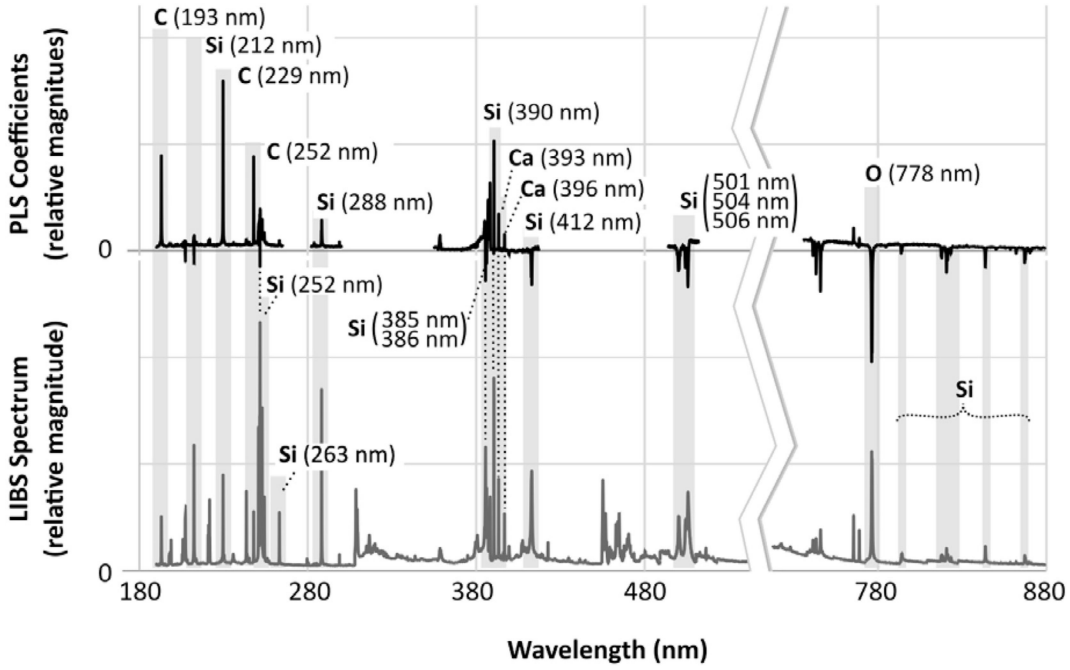

Fig. 8.

Plot of regression coefficients from the PLS model for TC (top) with a representative spectrum for DPM (from 5 kW engine load) below.

Table 1

Calibration, validation and prediction values for the test and validation sets of DPM samples.

Species	R^2_{cal}	RMSEC	RMSECV	R^2_{pred}	RMSEP	BIAS	RPD	RER
EC	0.9869	1.5764	2.0246	0.9635	1.8910	0.4418	5.3548	17.5344
OC	0.9200	3.2536	4.0706	0.6177	4.1780	0.5819	1.6553	5.7744
TC	0.9874	2.7660	3.6896	0.9305	4.2276	1.0237	3.8814	13.3764